Test of Equivalence Principle at 10^{-8} Level by a Dual-Species Double-Diffraction Raman Atom Interferometer

Lin Zhou,[1,2] Shitong Long,[1,2,3] Biao Tang,[1,2] Xi Chen,[1,2] Fen Gao,[1,2] Wencui Peng,[1,2] Weitao Duan,[1,2,3] Jiaqi Zhong,[1,2] Zongyuan Xiong,[1,2] Jin Wang,[1,2,*] Yuanzhong Zhang,[4] and Mingsheng Zhan[1,2,†]

[1]*State Key Laboratory of Magnetic Resonance and Atomic and Molecular Physics, Wuhan Institute of Physics and Mathematics, Chinese Academy of Sciences - Wuhan National Laboratory for Optoelectronics, Wuhan 430071, China*

[2]*Center for Cold Atom Physics, Chinese Academy of Sciences, Wuhan 430071, China*

[3]*University of Chinese Academy of Sciences, Beijing 100049, China*

[4]*Institute of Theoretical Physics, Chinese Academy of Sciences, Beijing 100190, China*

(Received 1 March 2015; published 2 July 2015)

We report an improved test of the weak equivalence principle by using a simultaneous ^{85}Rb-^{87}Rb dual-species atom interferometer. We propose and implement a four-wave double-diffraction Raman transition scheme for the interferometer, and demonstrate its ability in suppressing common-mode phase noise of Raman lasers after their frequencies and intensity ratios are optimized. The statistical uncertainty of the experimental data for Eötvös parameter η is 0.8×10^{-8} at 3200 s. With various systematic errors corrected, the final value is $\eta = (2.8 \pm 3.0) \times 10^{-8}$. The major uncertainty is attributed to the Coriolis effect.

DOI: 10.1103/PhysRevLett.115.013004 PACS numbers: 37.25.+k, 03.75.Dg, 04.80.Cc

The equivalence principle including the weak equivalence principle (WEP), also known as the universality of free fall, is one of the two assumptions of Einstein's general relativity. Theories which try to unify gravity and the standard model, generally require violation of WEP [1]. To explore the applicable extent of WEP and to help the birth of new quantum gravity theories, it is very important to precisely test WEP both with macro-objects and with microscopic particles. WEP has been tested experimentally with large objects by lunar laser ranging [2] and torsion balances [3] at 10^{-13} level, while with atoms it is tested only at 10^{-7} level.

The test with atoms relies on atom interferometry which has been developed for over 20 years [4] and has been widely used in measurements of gravity [5] and its gradient [6], the Newtonian gravitational constant [7], gravitational redshift [8], and post-Newtonian gravity [9]. Fray *et al.* [10] performed the first atom based WEP test using an atom interferometer (AI) with an Eötvös value of $\eta = (1.2 \pm 1.7) \times 10^{-7}$ by measuring the gravitational accelerations of the isotopic ^{85}Rb and ^{87}Rb atoms. Ten years later, Bonnin *et al.* [11] reported the same test to a similar accuracy of $\eta = (1.2 \pm 3.2) \times 10^{-7}$ by using simultaneous dual-species (^{85}Rb and ^{87}Rb) AIs. A nonisotopic pair of atoms, ^{87}Rb and ^{39}K, was also used recently by Schlippert *et al.* [12], they tested WEP with $\eta = (0.3 \pm 5.4) \times 10^{-7}$. In addition, the bosonic and fermionic isotopes of strontium atoms were also used to test WEP, the value is $(0.2 \pm 1.6) \times 10^{-7}$ [13].

On the other hand, a current single-species AI technique has reached very high resolution [14,15], which could principally push the AI based WEP test to a much higher accuracy than 10^{-7}. The main obstacles are complex noise that is difficult to be common-mode rejected, and crosstalk of different laser frequencies in a dual-species AI.

Here, we propose a simultaneous dual-species double-diffraction Raman AI and demonstrate a new WEP test with it. We design and realize a four-wave double-diffraction Raman transition (4WDR) scheme by carefully selecting the frequencies and intensity ratio of Raman beams to avoid the crosstalk among different lasers. The 4WDR scheme is based on the single-species double-diffraction Raman AI [16–18], but extended to two species (^{85}Rb and ^{87}Rb).

Our 4WDR scheme [19] is illustrated in Fig. 1. Raman beams for the dual-species AI are composed of four lasers with frequencies of ω_i and wave vectors $k_i (i = 1\text{–}4)$. ω_1 and ω_2 are used as shared Raman beams for ^{85}Rb and ^{87}Rb atoms, while ω_3 and ω_4 are for ^{85}Rb and ^{87}Rb, respectively. Pairs (ω_1, ω_3) and (ω_2, ω_3) are for a double-diffraction Raman transition of ^{85}Rb AI, while (ω_1, ω_4) and (ω_2, ω_4) are for ^{87}Rb.

In the 4WDR scheme, the frequencies and intensity ratios of Raman beams are chosen to meet the following requirements. (1) The four frequencies are far off resonant to all of the resonance lines of rubidium isotopes. (2) The intensities of two chirp lasers (ω_1 and ω_2) are equal, to ensure that the corresponding Rabi frequencies of two counter-propagated wave vectors in each double-diffraction Raman transition are equal, and atoms recoil to two interference paths with the same probability. (3) The corresponding Rabi frequencies of different species' AIs are the same. (4) For dual-species Raman transitions, the total ac Stark shift caused by four Raman beams is zero.

To find the optimal parameters, we calculate the ac Stark shift spectrum of rubidium atoms [see Fig. 1(a)]. To cancel ac Stark shifts in both species' AIs, some Raman frequencies should lie between the cooling laser ($F = 3$ to F') and repumping laser ($F = 2$ to F') for ^{85}Rb atoms. The

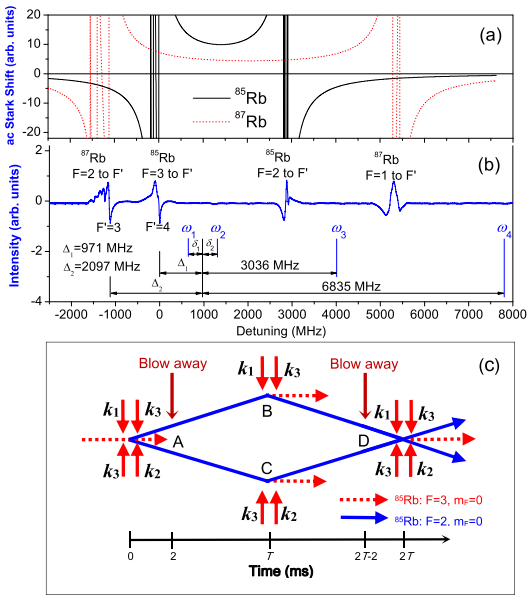

FIG. 1 (color online). Schematic diagram of the 4WDR scheme. (a) ac Stark shift spectrum of rubidium atoms. (b) Lasers with frequencies of $\omega_i (i = 1\text{–}4)$ are used as Raman beams for ^{85}Rb-^{87}Rb dual-species AI; δ_1 is the detuning of ω_1, δ_2 is the detuning of ω_2. ω_1 and ω_2 are detuned to the blue side of transitions $F = 3$ to $F' = 4$ of ^{85}Rb and $F = 2$ to $F' = 3$ of ^{87}Rb. (c) Diagram of a double-diffraction Raman AI using k_1, k_2, and k_3. The internal states of atoms don't change during the double diffraction Raman interferometric process, but the states are $\pm k_{\text{eff}}$ shifted in momentum.

frequencies of Raman beams we selected are shown in Fig. 1(b); they satisfy the following relation:

$$\omega_1 + \delta_1 = \omega_2 - \delta_2 = \omega_3 - 3.036\ \text{GHz} = \omega_4 - 6.835\ \text{GHz}, \quad (1)$$

where δ_i is the detuning of $\omega_i (i = 1, 2)$. $\delta_1 = \delta_2 = \upsilon k_{\text{eff}}/4\pi$, where υ is the projection of atomic velocity along the direction of the wave vector, $k_{\text{eff}} = k_1 + k_2 + 2k_3$ (for ^{85}Rb) or $k_1 + k_2 + 2k_4$ (for ^{87}Rb) are the effective wave vectors of the Raman lasers, and $\upsilon k_{\text{eff}}/4\pi$ equals the Doppler shift of atoms. Shown in the upper row of Fig. 1(b) is a polarization spectrum of rubidium atoms [20] for reference. By fixing the above frequency locations, we then decide the intensities. We find that the optimal intensity ratios of four Raman beams are $I_1 : I_2 : I_3 : I_4 = 1.0 : 1.0 : 3.1 : 14.3$, where I_i is the intensity of $\omega_i (i = 1\text{–}4)$.

A pronounced advantage of the 4WDR scheme is its capability to suppress the common mode phase noise of Raman lasers. This can be seen by writing the total phase shift [23] of a single-species [taking ^{85}Rb as an example and shown in Fig. 1(c)] double-diffraction Raman [19] AI

$$\Delta\varphi = k_{\text{eff}} g T^2 + \Delta\varphi_B + \Delta\varphi_C - \Delta\varphi_A - \Delta\varphi_D, \quad (2)$$

where T is the time interval of $\pi/\sqrt{2} - \sqrt{2}\pi - \pi/\sqrt{2}$ Raman pulse sequence [17], $\Delta\varphi_j$ $(j = A - D)$ is the initial phase shift at site j. Since Raman pairs (k_1, k_3) and (k_2, k_3) supply recoil momentum in opposite directions, the atom interference loop formed by the Raman pulse sequence is spatially symmetric [18]. By careful calculation, we find that the initial phases of k_3 are canceled due to the opposite recoil process in the interference loop, and the phase shift of each site only depends on the initial phases φ_{i0}^j of $k_i (i = 1, 2)$, i.e.,

$$\Delta\varphi_j = \varphi_{20}^j - \varphi_{10}^j (j = A\text{–}D). \quad (3)$$

Similarly, for ^{87}Rb atoms, the total phase shift of lasers is independent of k_4, and it is only sensitive to $\varphi_{i0}^j (i = 1, 2)$. In other words, the 4WDR scheme is immune to phase noises of both k_3 and k_4. The residual noise of φ_{i0}^j $(i = 1, 2)$ can be common-mode rejected since ^{85}Rb and ^{87}Rb AIs share the same k_1 and k_2.

The experimental setup [24] is a modified version of our early AIs [21,25]. As shown in Fig. 2, the magneto-optical trap (MOT) chamber is at the bottom of the setup and on the top is the fountain pipe, in between is the detection chamber. A pair of rectangular windows for two parallel probe beams are arranged along the horizontal direction of the detection chamber. Two round windows (window A, window B) are perpendicular to the axial of the two rectangular windows, they are used for collecting laser-induced fluorescence from ^{85}Rb and ^{87}Rb simultaneously for each shot of the fountain. Window A is 30 mm higher than window B. All laser beams are supplied by the laser system, which is composed of a seed laser, a taped laser amplifier, and some acousto-optic modulators (AOMs). The seed laser is stabilized by saturated absorption spectroscopy and its frequency is shifted by AOMs. The blue detuning of Raman beams [19] are realized by an electro-optic modulator [20].

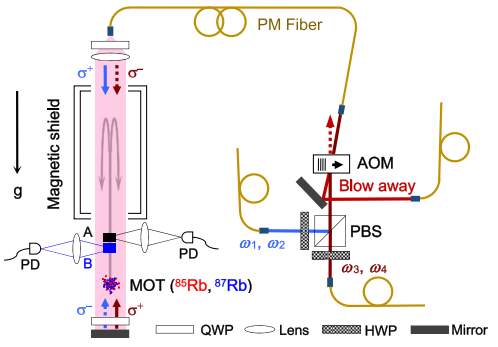

FIG. 2 (color online). Schematic diagram of experimental setup. Cold atoms trapped in MOT are launched up by moving molasses to form fountains. Raman beams and blow away beam are transited to interference area via single-mode polarization maintain fibers. Population signal of atoms are detected at window A and window B, simultaneously. HWP, half-wave plate; QWP, quarter-wave plate; PBS, polarization beam splitter; PM, polarization maintain; MOT, magneto-optical trap; AOM, acousto-optic modulator; PD, photon detector.

Cold ^{85}Rb and ^{87}Rb atom clouds are prepared in the MOT, and then launched simultaneously by a moving molasses process to form atom fountains. During the launching and falling process the 4WDR pulse sequence is applied. At the end, ^{85}Rb and ^{87}Rb are detected parallelly at window A and window B. By scanning δ_1 and δ_2 simultaneously at chirp rates of α_1 and α_2, respectively, the phase shifts of ^{87}Rb AIs are obtained, the phase shifts of ^{85}Rb AIs are obtained by the same way. By switching the frequencies of two probe beams, ^{87}Rb and ^{85}Rb atoms in window B and window A are detected alternately.

To evaluate the ability of phase noise suppression of the 4WDR scheme, a comparison experiment is performed. First, we shut off the Raman beam with a frequency of ω_2, and carry out simultaneous ^{85}Rb-^{87}Rb dual-species atom interferometry experiments by the usual single-diffraction Raman transitions method. An AOM driven by a triangle wave is used to modulate the phase of ω_3 to introduce rapid phase change to ^{85}Rb atoms. The experimental data are shown in Fig. 3(a). Because of the complicated phase variance from the modulation, ^{85}Rb atom interference fringes disappear, while the visibility of unperturbed ^{87}Rb atom interference fringes is 48%. As a comparison, we then switch on the Raman beam of ω_2, thus, the AI is in a double-diffraction configuration. The visibility of ^{85}Rb atom interference fringes, as shown in Fig. 3(b), is now about 20%, even if it is still suffering from the phase modulation of ω_3.

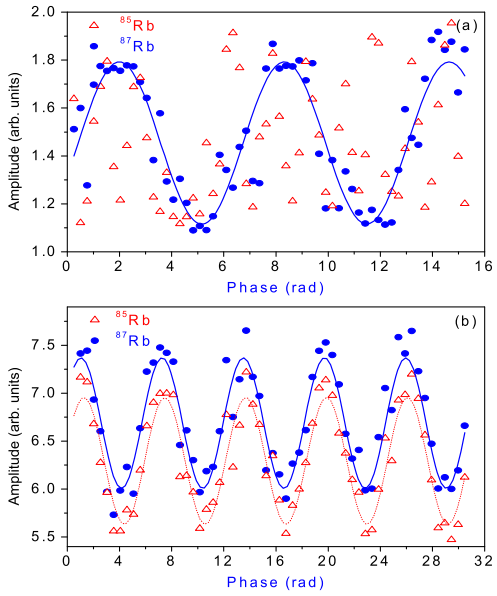

FIG. 3 (color online). Phase noise suppression by the 4WDR method. A rapid phase modulation is applied to ^{85}Rb atoms. (a) Simultaneous ^{85}Rb-^{87}Rb interference fringes obtained by single-diffraction Raman transition method and (b) simultaneous ^{85}Rb-^{87}Rb interference fringes by the 4WDR scheme. The red triangles are experimental data points of ^{85}Rb atoms, and the red dotted line is a sine curve fitting. The blue dots are experimental data points of ^{87}Rb atoms, and the blue solid line is a sine curve fitting.

This visibility is comparable with that of ^{87}Rb atoms. Meanwhile, as already demonstrated in [17,18], the phase sensitivity of interference fringes obtained by the 4WDR method is improved by two times [see Fig. 3(b)].

By using the 4WDR Raman AI we made gravity differential measurements. For each fringe, we repeat 40 measurements, and a single measurement lasts 2.5 s. By sine curve fitting, we determine the chirp rates corresponding to the centers of fringes; they are $\alpha_{85} = 2 \times 25.104\,08$ MHz/s for ^{85}Rb atoms and $\alpha_{87} = 2 \times 25.104\,20$ MHz/s for ^{87}Rb atoms, respectively. The difference is mainly caused by the difference of effective wave vectors.

To obtain the phase difference between ^{85}Rb and ^{87}Rb simultaneous interference fringes, we conducted ellipse fitting by setting interference fringe data of ^{85}Rb as x, ^{87}Rb as y [see Fig. 4(a) for a typical fringe data]. The value of $g_{85} - g_{87}$ is obtained by differential measurements [19] based on ellipse fitting. For an ellipse fitting, the smallest error occurs if the data distribution is close to a perfect circle, where the phase difference is $(2n+1)\pi/2$, n $(= 0; 1; 2; \ldots)$ is an integer. The value of $\Delta\varphi$ depends on experimental parameters T, k_{eff}, α_1, and α_2. For given k_{eff}, α_1, and α_2, $\Delta\varphi$ can only be determined by T. We set $T = 70.96$ ms, and the corresponding fitted phase difference is near $5\pi/2$. The frequency difference between ω_3 and ω_4 causes a systematic error of $-494.4 \times 10^{-8} g$ in gravity differential measurement; we also call this effective wave vector error.

We obtained two sets of data. Data A are fitted values of $g_{85} - g_{87}$ by probing ^{87}Rb atoms at window A while probing ^{85}Rb atoms at window B; data B are $g_{85} - g_{87}$ by probing ^{85}Rb at window A and ^{87}Rb at window B. The average of data A and data B is $-491.6 \times 10^{-8} g$. Two sets of data after correcting system errors are shown in Fig. 4(b), the average value of $g_{85} - g_{87}$ is $2.8 \times 10^{-8} g$. The relative gravity difference (namely, the Eötvös parameter) can be obtained by

$$\eta = \frac{(g_{85} - g_{87})}{(g_{85} + g_{87})/2}. \tag{4}$$

The Allan deviation of measurements for η is shown in Fig. 5. The deviation value σ_η in the dual-logarithm chart decreases at the square root of averaging time τ. At $\tau = 3200$ s, the deviation is 0.8×10^{-8}. The well-behaved Allan deviation indicates that white noise is the dominant noise source in the experiment. This, again, shows that the 4WDR scheme has good common-mode noise suppression ability, at least as demonstrated here at the 10^{-8} level.

To give an uncertainty budget of errors other than the direct experimental measurement, i.e., type B errors, we make the following estimates. The frequency difference between ω_3 and ω_4 is still a major systematic error, but because the uncertainty of laser frequency difference is less than 10 Hz, the uncertainty to correct the error is only 3×10^{-11}. The fluctuation of bias magnetic field in our experiment is less than 1 mG, so the uncertainty of η due to

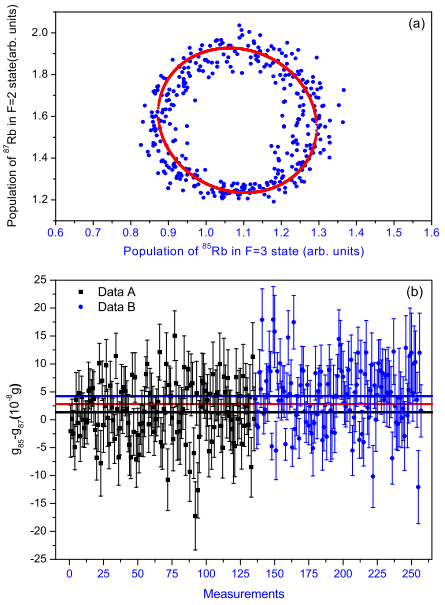

FIG. 4 (color online). Population of ^{87}Rb in $F = 2$ state vs population of ^{85}Rb in $F = 3$ state (a) and data for gravity differential measurements (b). The systematical error caused by the difference of effective wave vectors of ^{85}Rb and ^{87}Rb is corrected. Data A are obtained by probing ^{87}Rb atoms at window A while probing ^{85}Rb atoms at window B; data B are obtained by altering the probe position. The black line and the blue line are the average values of data A and data B, respectively. The average of data A and data B is $2.8 \times 10^{-8} g$ shown as a red line.

a second order Zeeman shift is less than 1×10^{-10}. Because of the tiny, but not zero, difference of ^{85}Rb and ^{87}Rb atoms in mass, launch velocity and recoil velocity, the central positions of two species' atom clouds are not completely overlapped during the free falling process. The Coriolis effect caused by Earth's rotation coupling with free falling atoms due to their horizontal velocity distribution, the fluctuations of initial positions, and velocities of two species' atoms, is another uncertainty source of the Eötvös parameter. The uncertainty of the horizontal position difference of two clouds is less than 2 mm, and the uncertainty of velocity difference is less than 1 mm/s. Considering the latitude of our laboratory (north latitude 30.54°), the calculated uncertainty caused by the Coriolis effect is 2.9×10^{-8}. The vertical position difference of ^{85}Rb and ^{87}Rb atom clouds is 0.23 ± 1.00 mm, thus, the gravity gradient based systematic error is less than 7×10^{-11}, and its uncertainty is 3×10^{-10}. In our experiments, the fluctuation of laser intensities is less than 10%; the uncertainty of η due to ac Stark shifts is measured in independent experiments to be less than 2×10^{-9}.

All above mentioned main contributions affecting the differential acceleration measurement are listed in Table I. Including all statistical uncertainties or errors (type A and type B) together, the total uncertainty of η value is 3.0×10^{-8}.

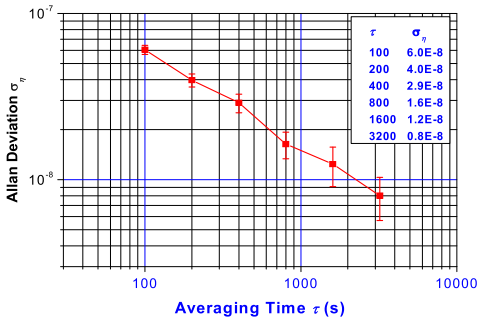

FIG. 5 (color online). Allan deviation of differential gravity measurement data of ^{85}Rb and ^{87}Rb atoms. The deviation of averaging 3200 s is 0.8×10^{-8}.

To further reduce the uncertainty, the Coriolis effect should be canceled. It can be done by rotating the mirrors [26] reflecting Raman beams. Then, the signal to noise ratio should be increased in our experiment by evolving more and further cooled atoms, and by suppressing residual noises like seismic vibration with active vibration isolation [27]. Finally, the 10-m fountain AIs [15,24] or even AI in space [28] will come to play with their ultrahigh sensitivity. All these efforts will, step by step in the long term, lead the AI-based WEP test to approach the limitation of Eötvös ratio of 10^{-13} or better [14,28,29], which is comparable to the classical torsion balance experiments.

In summary, we developed a simultaneous dual-species (^{85}Rb-^{87}Rb) cold AI in which the proposed 4WDR scheme was used and demonstrated to have obvious advantages in immunizing common-mode noises. The 4WDR AI carries forward all features, including a larger interference loop, better phase sensitivity, and suppression of the phase noises of external fields, revealed in single species counterpart. It also holds the new ability of suppressing common-mode phase noise of Raman lasers in the dual-species case. With this new type AI, we made a new WEP test at the 10^{-8} level and found no violation to the WEP. This work advances WEP testing with atoms a step forward by improving the accuracy about one order. Although different test mass combinations may have different sensitivity to the EP violation, and different theoretical models give various predictions, the improvement to the bounds on the violation parameters [30,31] with the (^{85}Rb-^{87}Rb) pair is straightforward.

TABLE I. Main contributions affecting the differential gravitational acceleration measurement.

	η ($\times 10^{-8}$)	Uncertainty ($\times 10^{-8}$)
Experimental data	−491.6	0.8
Effective wave vector error	−494.4	0.0
Second order Zeeman shift	0	0.01
Gravity gradient	0.01	0.03
Coriolis effect	0	2.9
ac Stark shift	0	0.2
Total	2.8	3.0

We thank Jun Luo, Tianchu Li, and Jun Ye for their helpful discussions and suggestions in error evaluation and data analysis. This work was supported by the National Natural Science Foundation of China under Grants No. 11227803 and No. 91436107, by the National Basic Research Program of China under Grant No. 2010CB832805, and also by funds from the Chinese Academy of Sciences.

*wangjin@wipm.ac.cn
†mszhan@wipm.ac.cn

[1] M. W. Clifford, The confrontation between general relativity and experiment, Living Rev. Relativity **9**, 3 (2006).
[2] J. G. Williams, S. G. Turyshev, and D. H. Boggs, Progress in Lunar Laser Ranging Tests of Relativistic Gravity, Phys. Rev. Lett. **93**, 261101 (2004).
[3] S. Schlamminger, K. Y. Choi, T. A. Wagner, J. H. Gundlach, and E. G. Adelberger, Test of the Equivalence Principle Using a Rotating Torsion Balance, Phys. Rev. Lett. **100**, 041101 (2008).
[4] A. D. Cronin, J. Schmiedmayer, and D. E. Pritchard, Optics and interferometry with atoms and molecules, Rev. Mod. Phys. **81**, 1051 (2009).
[5] Y. Bidel, O. Carraz, R. Charriere, M. Cadoret, N. Zahzam, and A. Bresson, Compact cold atom gravimeter for field applications, Appl. Phys. Lett. **102**, 144107 (2013).
[6] F. Sorrentino, Q. Bodart, L. Cacciapuoti, Y. H. Lien, M. Prevedelli, G. Rosi, L. Salvi, and G. M. Tino, Sensitivity limits of a Raman atom interferometer as a gravity gradiometer, Phys. Rev. A **89**, 023607 (2014).
[7] G. Rosi, F. Sorrentino, L. Cacciapuoti, M. Prevedelli, and G. M. Tino, Precision measurement of the Newtonian gravitational constant using cold atoms, Nature (London) **510**, 518 (2014).
[8] H. Müller, A. Peters, and S Chu, A precision measurement of the gravitational redshift by the interference of matter waves, Nature (London) **463**, 926 (2010).
[9] H. Müller, S. W. Chiow, S. Herrmann, S. Chu, and K. Y. Chung, Atom-Interferometry Tests of the Isotropy of Post-Newtonian Gravity, Phys. Rev. Lett. **100**, 031101 (2008).
[10] S. Fray, C. A. Diez, T. W. Hänsch, and M. Weitz, Atomic Interferometer with Amplitude Gratings of Light and its Applications to Atom Based Tests of the Equivalence Principle, Phys. Rev. Lett. **93**, 240404 (2004).
[11] A. Bonnin, N. Zahzam, Y. Bidel, and A. Bresson, Simultaneous dual-species matter-wave accelerometer, Phys. Rev. A **88**, 043615 (2013).
[12] D. Schlippert, J. Hartwig, H. Albers, L. L. Richardson, C. Schubert, A. Roura, W. P. Schleich, W. Ertmer, and E. M. Rasel, Quantum Test of the Universality of Free Fall, Phys. Rev. Lett. **112**, 203002 (2014).
[13] M. G. Tarallo, T. Mazzoni, N. Poli, D. V. Sutyrin, X. Zhang, and G. M. Tino, Test of Einstein Equivalence Principle for 0-Spin and Half-Integer-Spin Atoms: Search for Spin-Gravity Coupling Effects, Phys. Rev. Lett. **113**, 023005 (2014).
[14] S. Dimopoulos, P. W. Graham, J. M. Hogan, and M. A. Kasevich, Testing General Relativity with Atom Interferometry, Phys. Rev. Lett. **98**, 111102 (2007).
[15] S. M. Dickerson, J. M. Hogan, A. Sugarbaker, D. M. S. Johnson, and M. A. Kasevich, Multiaxis Inertial Sensing with Long-Time Point Source Atom Interferometry, Phys. Rev. Lett. **111**, 083001 (2013).
[16] B. Dubetsky and P. R. Berman, $\lambda/8$-period optical potentials, Phys. Rev. A **66**, 045402 (2002).
[17] T. Lévèque, A. Gauguet, F. Michaud, F. Pereira Dos Santos, and A. Landragin, Enhancing the Area of a Raman Atom Interferometer Using a Versatile Double-Diffraction Technique, Phys. Rev. Lett. **103**, 080405 (2009).
[18] N. Malossi, Q. Bodart, S. Merlet, T. Lévèque, A. Landragin, and F. Pereira Dos Santos, Double diffraction in an atomic gravimeter, Phys. Rev. A **81**, 013617 (2010).
[19] See Supplemental Material at http://link.aps.org/supplemental/10.1103/PhysRevLett.115.013004 for a detailed description of the 4WDR scheme, Raman laser system, 4WDR process, and differential measurements, which includes Refs. [20–22].
[20] W. C. Peng, L. Zhou, S. T. Long, J. Wang, and M. S. Zhan, Locking laser frequency of up to 40 GHz offset to a reference with a 10 GHz electro-optic modulator, Opt. Lett. **39**, 2998 (2014).
[21] L. Zhou, Z. Y. Xiong, W. Yang, B. Tang, W. C. Peng, Y. B. Wang, P. Xu, J. Wang, and M. S. Zhan, Measurement of local gravity via a cold atom interferometer, Chin. Phys. Lett. **28**, 013701 (2011).
[22] G. T. Foster, J. B. Fixler, J. M. McGuirk, and M. A. Kasevich, Method of phase extraction between coupled atom interferometers using ellipse-specific fitting, Opt. Lett. **27**, 951 (2002).
[23] M. Kasevich and S. Chu, Measurement of the gravitational acceleration of an atom with a light-pulse atom interferometer, Appl. Phys. B **54**, 321 (1992).
[24] L. Zhou, Z. Y. Xiong, W. Yang, B. Tang, W. C. Peng, K. Hao, R. B. Li, M. Liu, J. Wang, and M. S. Zhan, Development of an atom gravimeter and status of the 10-meter atom interferometer for precision gravity measurement, Gen. Relativ. Gravit. **43**, 1931 (2011).
[25] P. Wang, R. B. Li, H. Yan, J. Wang, and M. S. Zhan, Demonstration of a Sagnac type cold atom interferometer with stimulated raman transitions, Chin. Phys. Lett. **24**, 27 (2007).
[26] S. Y. Lan, P. C. Kuan, B. Estey, P. Haslinger, and H. Müller, Influence of the Coriolis Force in Atom Interferometry, Phys. Rev. Lett. **108**, 090402 (2012).
[27] B. Tang, L. Zhou, Z. Y. Xiong, J. Wang, and M. S. Zhan, A programmable broadband low frequency active vibration isolation system for atom interferometry, Rev. Sci. Instrum. **85**, 093109 (2014).
[28] D. N. Aguilera, H. Ahlers, B. Battelier *et al.*, STE-QUEST-test of the universality of free fall using cold atom interferometry, Classical Quantum Gravity **31**, 115010 (2014).
[29] J. Hartwig, S. Abend, C. Schubert, D. Schlippert, H. Ahlers, K. Posso-Trujillo, N. Gaaloul, W. Ertmer, and E. M. Rasel, Testing the universality of free fall with rubidium and ytterbium in a very large baseline atom interferometer, New J. Phys. **17**, 035011 (2015).
[30] T. Damour, Theoretical aspects of the equivalence principle, Classical Quantum Gravity **29**, 184001 (2012).
[31] V. A. Kostelecky and J. D. Tasson, Matter-gravity couplings and Lorentz violation, Phys. Rev. D **83**, 016013 (2011).